Journal of Neuroscience Methods 176 (2009) 230–236

Contents lists available at ScienceDirect

Journal of Neuroscience Methods

journal homepage: www.elsevier.com/locate/jneumeth

High spatiotemporal resolution imaging of the neurovascular response to electrical stimulation of rat peripheral trigeminal nerve as revealed by *in vivo* temporal laser speckle contrast

Nan Li[a], Xiaofeng Jia[a], Kartikeya Murari[a], Renuka Parlapalli[b], Abhishek Rege[a], Nitish V. Thakor[a,*]

[a] *Department of Biomedical Engineering, Johns Hopkins University School of Medicine, Baltimore, MD 21205, USA*
[b] *Department of Biomedical Engineering, the University of Texas at Arlington, Arlington, TX 76019, USA*

ARTICLE INFO

Article history:
Received 16 April 2008
Received in revised form 15 July 2008
Accepted 15 July 2008

Keywords:
Temporal laser speckle contrast imaging
Ridge tracking
Trigeminal nerve
Migraine
Vasomotor response
Blood flow
Neurovascular system

ABSTRACT

Previous studies have implicated the abnormal activation of the trigeminal system to be a factor in the pathogenesis of migraine. The relationship between vascular changes and migraine, however, is under considerable debate. In this study, temporal laser speckle contrast imaging is combined with ridge tracking based vessel detection to obtain high resolution (6.7 μm × 6.7 μm), high contrast images of cerebral vascular structure. For the first time, the vasomotor and blood flow responses to electrical stimulation in rat peripheral trigeminal system were obtained simultaneously. The system is capable of picking up individual vessels with diameters down to 30 μm. The spatial spread of the blood velocity response relative to the point of stimulation was studied. Analysis of branching vessels showed a 50 ± 5% vs. 30 ± 5% change in mean peak magnitude and a 54% per second vs. 17% per second change in mean rate of increase for vessels proximal vs. distal to the stimulation site. The penetration depth of the laser used was proven to be sufficient to image dural as well as cortical vessels through a thinned skull preparation. Different responses were observed from cortical and dural vessels. While the diameter of cortical vessels did not change in response to the stimulation the blood velocity went up by 65 ± 5% per second. Dural vessels enlarged by 40 ± 8% and the blood velocity increased by 50 ± 5%. The method described here could be very useful in understanding and studying disorders in the neurovascular system.

1. Introduction

Migraine is a common incapacitating disorder. One of the proposed mechanisms of migraine, still under active investigation, is that neural events cause vasodilation, which, in turn, results in pain and further abnormal activation of the trigeminal nerve system (Goadsby et al., 2002). Early studies have implicated the afferent input from the dura mater to be the neural substrate for headache (Penfield, 1940; Ray and Wolff, 1940) and hence the meningeal sensory innervation from the peripheral trigeminal nerves is a major focus in migraine research (Pietrobon and Striessnig, 2003; Strassman and Raymond, 1997). Abnormal activation of the peripheral trigeminal nerve is known to cause the release of Calcitonin Gene-related peptide (CGRP), neurokinin A, and substance P into the dural meningeal vessels which in turn cause vasodilation and plasma protein extravasation (Arulmozhi et al., 2005; Edvinsson and Goadsby, 1994b). However, the failure of vasoconstrictors like epinephrine to cure migraine indicates that vasodilation is not the only perturbation caused by neurogenic inflammation (Bergerot et al., 2006). Other vascular or blood circulation changes may also be responsible. Nevertheless, the relationship between vascular changes and migraine is controversial.

Most neurovascular models of migraine are focused on changes resulting from trigeminal nerve activation with electrical or chemical stimulation. Electrical stimulation of the peripheral trigeminal nerves is a mature model for the study of migraine (Ahn and Goadsby, 2006; Bergerot et al., 2006). Earlier studies have measured blood flow changes using Laser Doppler Flowmetry (LDF) (Shimazawa and Hara, 1996) and intravital microscopy for detecting vascular diameter(Williamson et al., 2001). These studies have looked at limited vessels, mainly branches of the middle meningeal artery (MMA), and failed to give an overall understanding of the different responses from dural and cortical vessels. The meningeal sensory fibers innervate major cerebral arteries, including pial arteries such as the middle cerebral artery that carry the blood

* Corresponding author at: Tralor 710B, 720 Rutland Avenue, Johns Hopkins University School of Medicine, Baltimore, MD 21205, USA. Tel.: +1 410 955 7093; fax: +1 410 502 9814.
E-mail address: nitish@jhu.edu (N.V. Thakor).

0165-0270/$ – see front matter © 2008 Elsevier B.V. All rights reserved.
doi:10.1016/j.jneumeth.2008.07.013

to the brain, as well as the dural venous sinus that carries blood away from the brain (Strassman and Levy, 2006). However, most of the current neurophysiological studies focus mainly on the dura. The lack of information about the responses from pial vessels represents a significant gap in the understanding of the role of meningeal innervation in migraine.

For cerebrovascular flow studies, most physiologists use LDF. However, LDF yields regional blood flow changes and cannot resolve flow in specific blood vessels. Magnetic resonance imaging (MRI), positron emission tomography (PET) and xenon computed tomography (XeCT) suffer both in terms of spatial resolution limited to about 100–500 μm (Weber et al., 2006; Wintermark et al., 2005) and in terms of limited use in continuous monitoring over extended periods of time. Methods involving microsphere introduction are mostly sacrificial (De Visscher et al., 2006), because they rely on the number of particles embolizing the capillaries of organs. Methods involving dye introduction, for the purpose of contrast enhancement or particle tracking, run the risk of altering the physiological environment (Hillman, 2007). Intravital microscopy, though used for vascular diameter detection, has relatively low contrast and temporal resolution (Williamson et al., 2001). To our knowledge, no previous study has simultaneously measured changes in vessel size and blood flow at the level of individual vessels.

Laser speckle imaging (LSI) is based on the analysis of dynamic interference patterns caused by moving particles such as red blood cells in a vessel. LSI requires a simple and inexpensive setup and offers images with high spatiotemporal resolution. At the same time, it provides a full-field, two-dimensional mapping of blood velocity without scanning. Most of the work using LSI has been focused on functional imaging, creating blood flow maps in tissues like the cortex, retina and skin and observing changes in blood velocity under various stimulations (Dunn et al., 2001; Ruth, 1994; Tamaki et al., 1994). In our previous work (Murari et al., 2007), we presented and quantified an improved temporal laser speckle imaging system (tLSI) to obtain contrast enhanced images of cerebral microvasculature in the rat cortex.

In this work we have tailored the tLSI system to study in detail the neurovascular response of the peripheral trigeminal system to electrical stimulation. By combining tLSI with the ridge tracking algorithm (Aylward and Bullitt, 2002) for vessel detection, we obtained, for the first time, simultaneous vasomotor and blood velocity responses. The wide-field nature of tLSI provided details of the spatial distribution of the vascular response to stimulation. We observed different dynamics in the vasomotor and blood flow responses of vessels in different spatial locations. Furthermore, the penetration depth of the imaging modality was demonstrated to be sufficient for imaging cortical and dural vessels at the same time. Contrasting responses of cortical and meningeal vessels were observed in this study.

2. Materials and methods

2.1. Temporal Laser speckle contrast

Speckle is a random field intensity pattern produced by the interference of coherent or partially coherent beams that are subject to minute temporal or spatial fluctuations (Goodman, 1976). These patterns are seen when monochromatic coherent light is incident on a rough surface or a field of scattering particles. If the field of particles is non-static, photographing the dynamic speckle pattern results in an image that is blurred over the exposure time of the recording device. The velocity information in the blur can be extracted and mapped to contrast using statistical arguments (Briers, 2001; Ohtsubo and Asakura, 1976). In particular, laser speckle contrast (C) can be defined as

$$C = \frac{\langle I_M^2 \rangle - \langle I_M \rangle^2}{\langle I_M \rangle^2} = \frac{\sigma_M^2}{\langle I_M \rangle^2} \quad (1)$$

where $\langle I_M \rangle$ and $\langle I_M^2 \rangle$ are the average and the mean-square values of the time-varying speckle intensity over M observations. σ_M^2 is the square of the standard deviation of the time-varying speckle intensity. For tLSI, the contrast C can be calculated over time using a time stack of images. In this case a 1×1 pixel window is moved across a time stack of M images to obtain the statistics leading to a temporally contrasted image.

The tLSI method relies on obtaining contrast images of vessels where intensity is inversely proportional to the blood velocity. The velocity of the scattering particles v and the speckle contrast C can be related through the integration time as follows (Ohtsubo and Asakura, 1976):

$$v = \frac{2w}{T} \frac{\langle I_M \rangle^2}{\langle I_M^2 \rangle - \langle I_M \rangle^2} = \frac{2w}{T} \frac{1}{C} \quad (2)$$

where T is the integration time and w is the radius of the illuminating beam.

2.2. Animal preparation

All experiments were performed using protocols approved by the Johns Hopkins Animal Care and Use Committee. Adult female Wistar rats (200–250 g) were anesthetized with an intraperitoneal injection of *3* ml/kg of sodium pentobarbitone. Rectal temperature was maintained at 37 °C throughout using a homeothermic blanket system. The rat was placed in a stereotactic frame (David Kopf Instruments, Tujunga, CA). The scalp was shaved and disinfected with 70% ethanol and povidone-iodine solution. All procedures were performed using standard sterile precautions. After a midline scalp incision, the galea and periosteum overlying the parietal bone bilaterally were swept and retracted laterally. A 5 mm × 5 mm area centered at 3.5 mm lateral to and 3 mm posterior to the bregma was thinned using a high speed dental drill (Fine Science Tools Inc. North Vancouver, Canada), until the inner cortical layer of bone was encountered and underlying Middle Meningeal Artery (MMA) was visualized.

2.3. Electrical stimulation

Peripheral trigeminal nerve stimulation was carried out by a programmed repetitive stimulus pattern. After completion of the thinned skull preparation as described above, a NEX200 bipolar stimulating electrode (Rhodes Medical Instruments, Summerland, CA) was mounted on the surface of the cranial window approximately 200 μm from the branch of interest of the MMA using a precision micromanipulator. The cranial window was covered with mineral oil to maintain moisture on the surface of the skull. Based on literature (Goadsby et al., 2002) and our own prior experience, the trigeminal fibers were stimulated with a 1 ms pulse train at 5 Hz for a duration of 10 s using a stimulator (Grass-Astro-Med. Inc., W. Warwick, RI). The stimulus current was chosen to be the smallest value that elicited reliable responses. In accordance with literature (Williamson et al., 2001) and our experimental experience, a current of 50 μA was found sufficient and used for all stimulation. We gave a rest period of about 20 min before the subsequent stimulation trials to allow the vessels to return to a baseline state.

2.4. Imaging setup and protocol

The stereotactic frame holding the rat was placed on a platform which could be moved along the x–y axes for precise localization of the region of interest. A red HeNe gas laser of wavelength 632 nm (JDSU, Milpitas, CA) was used to illuminate the cranial window for speckle imaging. For white light images, a DC powered halogen source (Pelican, Torrance, CA) was used. Images were acquired using a 12-bit cooled SVGA CCD camera (PCO, Kelheim, Germany). A 60 mm, f/2.8 macro-lens with a maximum reproduction ratio of 1:1 (Nikon Inc., Melville, NY) was mounted on the camera. For speckle imaging, once the magnification was set, the aperture was set to approximate the speckle size to the pixel size (6.7 μm × 6.7 μm) which is the optimal condition for photographing speckles (Yuan et al., 2005). Finally, the shutter speed was set to get an optimal exposure. Images were taken continuously at a rate of 10 fps.

For imaging the response to the electrical stimulation of peripheral trigeminal nerves, we continuously recorded images over a duration of 5 min. Each trial began with 10 s of baseline recording, followed by 10 s electrical stimulation and 300 s of recovery time. A complete session consisted of four trials. All raw image data were streamed to a computer for subsequent offline processing.

2.5. Image analysis

2.5.1. Blood flow calculation

A set of 40 consecutive frames of raw images was converted into one tLSI image according to Eq. (1). While this contrast computation conserves spatial resolution, it will cause a 40-fold loss of temporal information. To maintain high temporal resolution, we apply a sliding window along the time sequences of the raw images. Each raw laser image with time index i has its corresponding contrast image which is calculated from a timestack of M images with indices $i-19,\ldots,i,\ldots,i+20$. Thus, the temporal resolution of our algorithm is simply determined by the frame rate of the camera (10 fps in this work). However, for computational simplicity, we performed all processing offline instead of doing it real-time. The intensity of each pixel in the speckle contrast image was used for calculating the relative blood flow velocity.

Most works in laser speckle contrast literature (Ayata et al., 2004; Cheng et al., 2003; Paul et al., 2006) simply relate the speckle contrast to cerebral blood flow whereas, in reality, it is related to the blood velocity (Briers, 1996; Ohtsubo and Asakura, 1976). Blood flow is defined as the volume of blood that is moving per unit of time and is measured in units of ml/min. Blood velocity, on the other hand, is the distance moved by a cell within the bloodstream per unit time and is measured in cm/s. The flow of blood in a vessel is related to velocity by the following equation:

$$F = VA \tag{3}$$

where F is the flow, V is the mean velocity, and A is the cross-sectional area of the vessel. Therefore, to estimate blood flows from the speckle contrast, both the blood velocity and the cross-sectional area of the vessel under consideration are needed.

2.5.2. Vessel size detection

As presented in our previous work (Murari et al., 2007), tLSI leads to a two to four fold increase in contrast to noise ratios (CNR), without the need for any contrast agents over white or green light reflectance imaging. This highly enhanced image quality enables

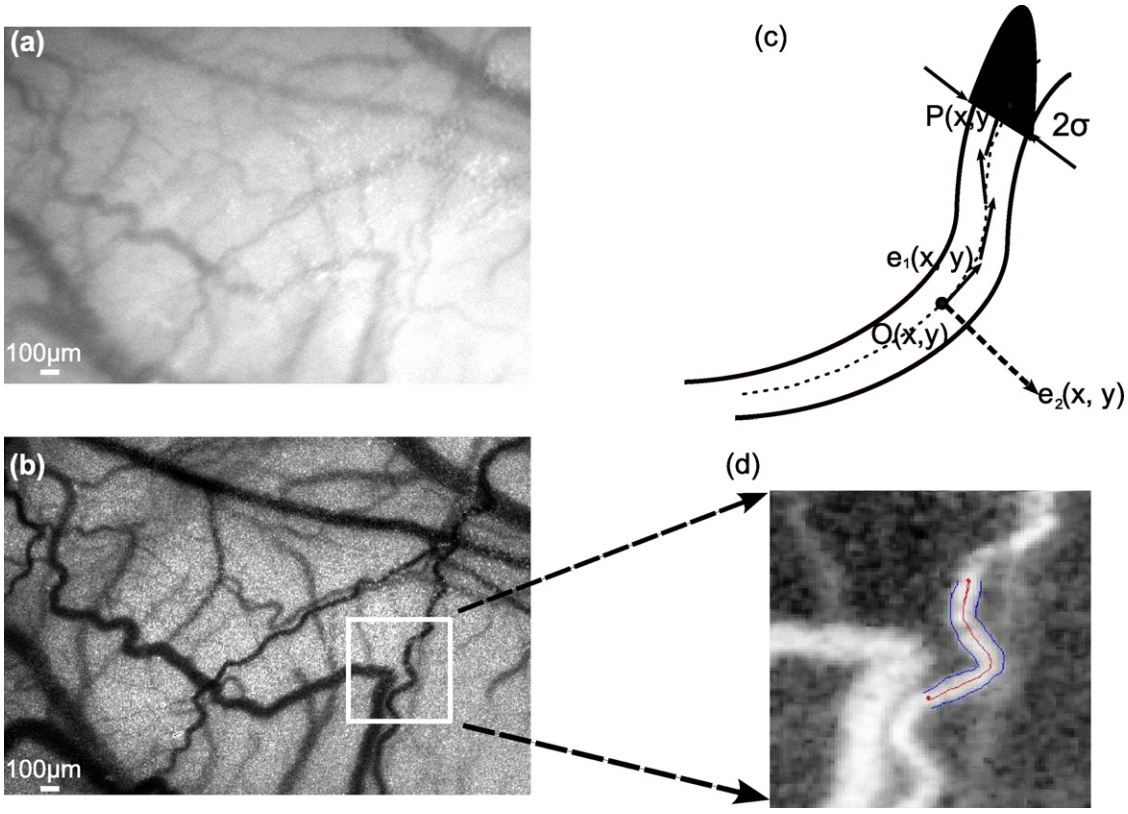

Fig. 1. Images of the same region of a rat brain obtained through a thinned skull using (a) white light reflectance imaging and (b) temporal laser speckle imaging (tLSI)obtained by calculating the temporal contrast across a stack of 40 images acquired sequentially in time. Note the higher contrast of the tLSI image and its potential to reveal more microvessels. (c) An illustration of the vessel diameter detection. 2σ is the estimated diameter of a point along the vessel which has the start point O(x, y) and end point P(x, y). The unit of σ is pixels. The real size of the vessel can be calculated knowing the pixel size. $e_2(x, y)$ and $e_1(x, y)$ are vectors normal and tangential to the vessel. (d) shows an example of diameter detection of a part of the individual vessel marked in (b).

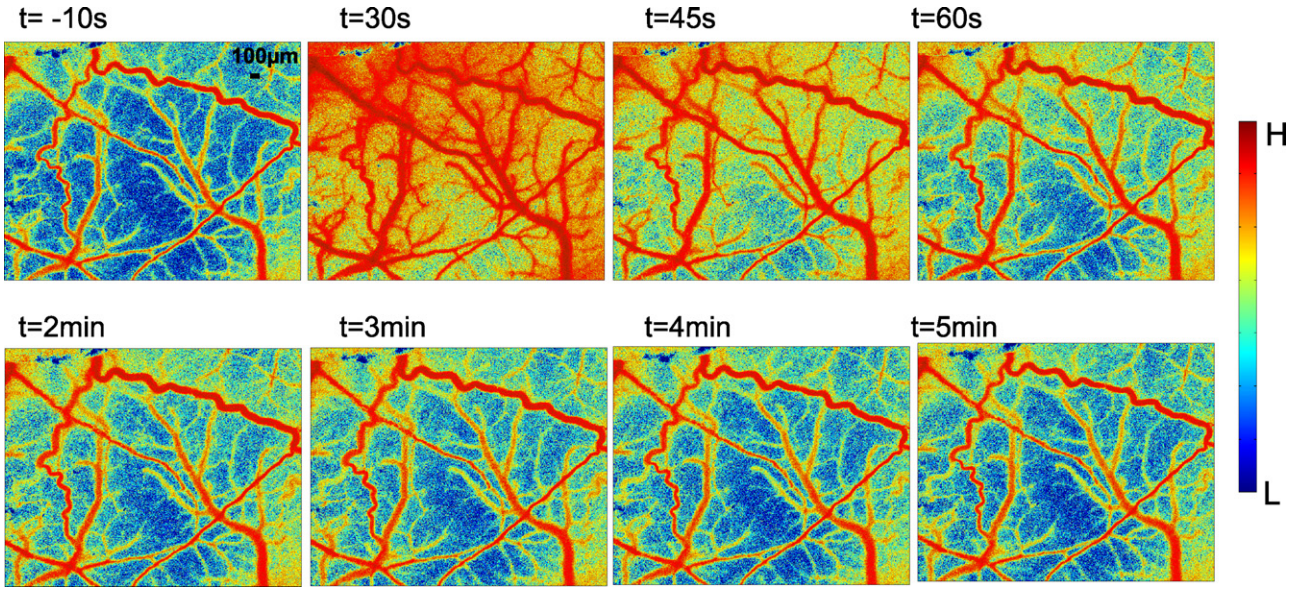

Fig. 2. Pseudo-color images displaying the vascular responses during and after electrical stimulation of peripheral trigeminal nerve fibers. The recording started at $t = -10$ s to obtain the baseline. The stimulation started at $t = 0$ s and continued for 10 s. The response was recorded throughout the stimulation for 300 s post-stimulation. The tissue perfusion and blood velocity increases from $t = 30$ s to $t = 60$ s and finally reduces back to baseline. Red and blue represent blood with the highest and lowest velocity, respectively.

the visualization of fine vascular structures. To estimate the size of individual vessels at a desired location, we segmented a small length of the vessel near the location, and took the mean value of the detected diameters at each pixel on the vessel-centerline. This is shown in Fig. 1(c) and (d). The segmentation method was based on the ridge tracking approach developed by Aylward et al.(Aylward et al., 1996). The method considers a 2D image as a surface in a 3D space by mapping intensity into height. Vessel centerlines exist as 1D surface maxima (ridges) on that surface. The segmentation process consists of finding ridge points and following them. The ridge start point O(x, y), start tangent direction $e_1(x, y)$, and end point P(x, y) were selected beforehand. The algorithm takes steps along the estimated ridge direction, shown by the dashed line, which is the medial axis of the vessel, and optimizes the medialness and diameter. $e_2(x, y)$ is the norm direction of the ridge at point O(x, y). 2σ is estimated to be the diameter at the current point being tracked along the vessel. An adaptive anisotropic diffusion filter was applied to the speckle contrast image before the segmentation to reduce the high frequency speckle noise (Yu and Acton, 2002).

3. Results

3.1. Vasomotor and blood flow response to stimulation

A white light image and a tLSI image of the same region through the thinned cranial window are shown in Fig. 1(a). The tLSI image shows much higher contrast for the major vessels and even for micro-vessels with diameters down to 30 μm. The intensity of the pixels in the tLSI image is inversely proportional to the blood velocity.

By analyzing the tLSI images, the tissue perfusion and vascular response under electrical stimulation of the peripheral trigeminal nerves were observed. Fig. 2 shows pseudo-color images in temporal sequence, displaying the responses during and after the electrical stimulation of the peripheral trigeminal nerve fibers, which intensely innervates the MMA and its branches in the dura mater. The colormap for the group of images was generated according to the grey level intensities in the tLSI images. Red represents the highest blood velocity with a grey level of 0, while blue represents the lowest velocity with grey level intensity of 1. The baseline tLSI image was acquired before stimulation. The stimulation was started at $t = 0$ s with a stimulation duration of 10 s. Image acquisition was started at $t = -10$ s to obtain the baseline and continued through the stimulation and was stopped 5 min post-stimulation. As observed from Fig. 2, the tissue perfusion and blood velocity increased from $t = 30$ to $t = 60$ s and then gradually decreased back towards the baseline value. The vessel size changes can be observed in the same image sequences. However, due to the small size of the vessels, vessel size changes were hard to be seen with the naked eye.

To quantitatively study the vasomotor and the blood flow response of the branches if the MMA, a region of interest (ROI) was chosen around a single vessel (Fig. 3(a)). The ridge tracking method was applied to a small part of the vessel to detect the vessel size. The experiment was repeated in six adult female Wistar rats. While the magnitude and latency of the response varied across animals, similar trends of the vascular response were observed among all animals. The changes were averaged from four trials on the same animal under the same experimental paradigm. In Fig. 3(b), the top panel shows that the blood velocity increased by up to $50 \pm 5\%$, and eventually decreased back to the baseline value. The middle panel shows the mean response of vessel diameter. Initially, a short constriction of the vessel was observed followed by a subsequent large dilation and a slow return to baseline. The dilation of the vessel size peaked at $40 \pm 8\%$. The percentage change in the blood flow in the same vessel is shown in the bottom panel of Fig. 3(b). The increase in the blood flow peaked at $80 \pm 15\%$. Error accumulation in Eq. (3) causes the standard deviation error in the blood flow to be higher than that in the blood velocity and the vessel diameter.

3.2. Spatial variation in the response to stimulation

The spatial spread of the blood velocity response relative to the point of stimulation was studied using the same experimental paradigm as above. Fig. 4 shows the experimental results from one animal averaged over four trials. P1 and P2 are locations along the

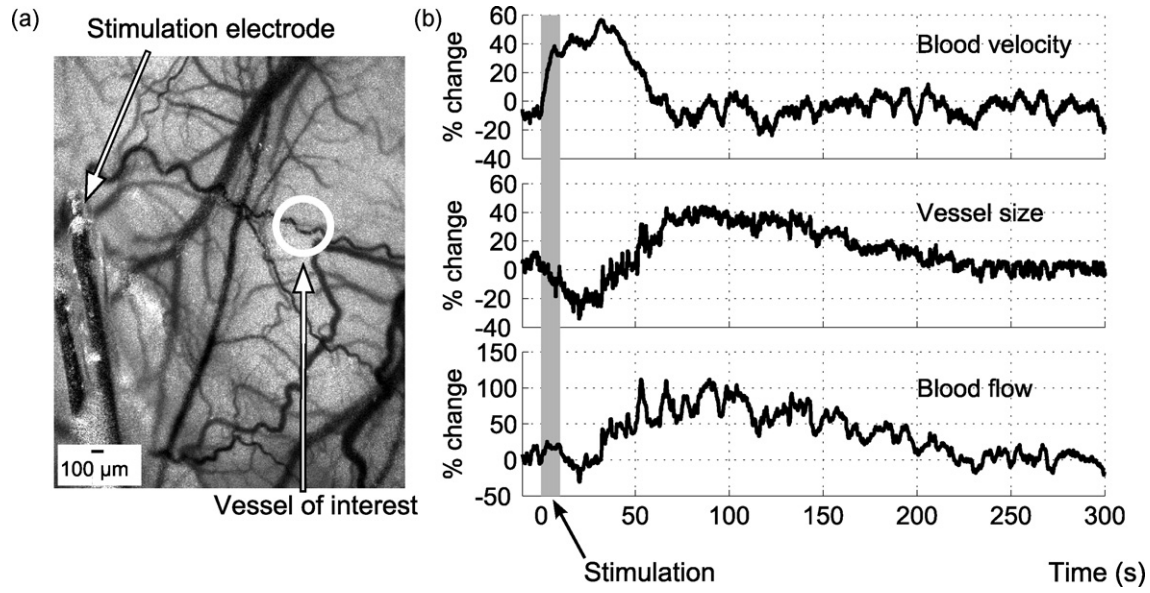

Fig. 3. Responses to electrical trigeminal stimulation. (a) Region of interest with the selected branch of the MMA marked. (b) Change in blood velocity (top panel) and vessel diameter (middle panel) of the selected branch detected using tLSI. The blood velocity increases and the diameter is also seen to increase after a short initial constriction. The blood flow changes (bottom panel) in the same vessel, calculated from the changes in both velocity and vessel diameter.

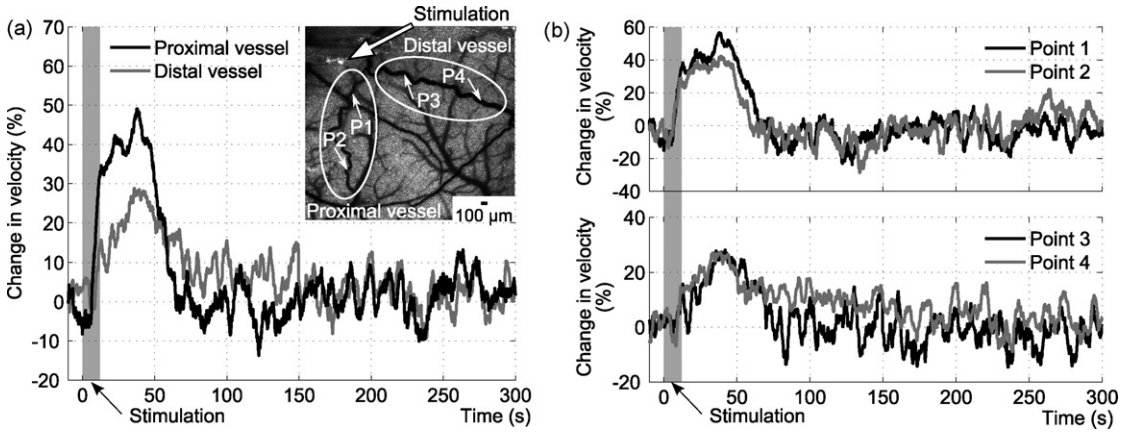

Fig. 4. Spatial spread of responses to electrical trigeminal stimulation. (a) Mean changes in the blood velocity in the proximal (black trace) and distal (grey trace) vessels. Data summarized in Table 1. The inset shows vessel branches proximal and distal to the stimulation location. (P1, P2) and (P3, P4) are points on the proximal and distal vessels, respectively. (b) Velocity changes at two different points on the proximal branch (top panel) and the distal branch (bottom panel). Black trace shows changes at points P1 (top panel) and P3 (bottom panel) and the grey trace shows changes at points P2 (top panel) and P4 (bottom panel).

vessel proximal to the stimulation site, marked inside the left white circle in Fig. 4(a). P3 and P4 are locations of the distal vessel on the right. There was no obvious difference in either the magnitude or the latency of the response along one individual vessel (Fig. 4(b)). However, the responses from the two vessels were quite distinct (Fig. 4(a)). Table 1 shows the mean rate of increase and the peak magnitude of the velocity change in the two vessels. Vessels proximal to the stimulation site responded quicker and showed greater response. The mean rate of increase was calculated over the time from within 10% of baseline to within 90% of the maximum. Similar trends were observed in the spread of response among all six animals studied.

Table 1
Comparison of the change in blood velocity in vessels proximal and distal stimulation location (inset in Fig. 4a) detected by tLSI ($n = 4$ trials).

Change in blood velocity	Proximal vessel	Distal vessel
Mean rate of increase	54% per second	17% per second
Peak magnitude	$50 \pm 5\%$	$30 \pm 5\%$

3.3. Stimulation effects on dural vs. cortical vessels

Next, we present a comparison of the responses from dural and cortical vessels to the electrical stimulation of the peripheral trigeminal nerves. Fig. 5 shows that the penetration depth of the 632 nm red laser was sufficient for imaging subdural cortical vessels through a thinned skull in a minimally invasive fashion. First, we followed the procedure from Section 2.2 to obtain speckle contrast images. After imaging through the thinned skull cranial window, the skull was opened, the dura was carefully excised, and a small metal chamber with removable glass cover-slip was glued to the skull. The space between the glass and the exposed cortex was filled with artificial cerebral spinal fluid. Using the same imaging protocol, a second speckle contrast image was obtained. Fig. 5(a) and (b) show the vasculature with and without the dura,

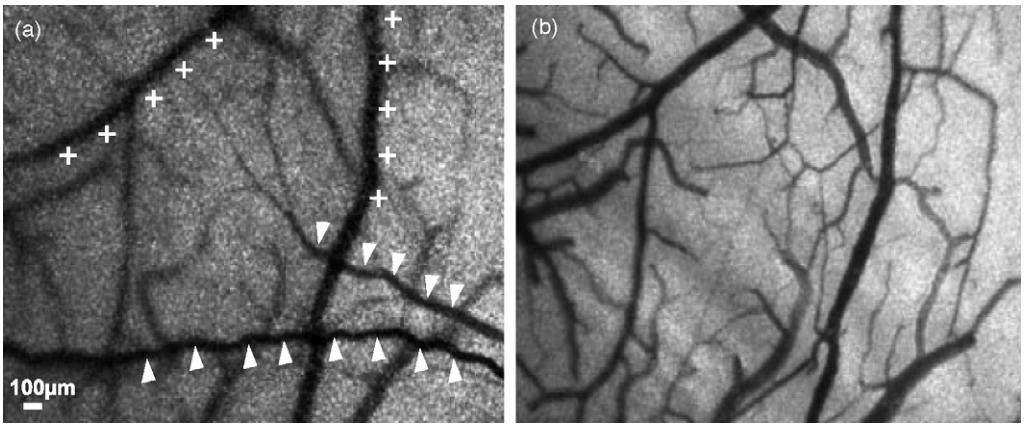

Fig. 5. Visualizing cortical vs. dural vessels using tLSI. Speckle images through a thinned skull (a) and after excising the dura (b). Vessels seen in both images (marked with '+') are cortical vessels while those seen only in the thinned skull image (marked with '△') are dural vessels.

respectively. Comparing the two tLSI images, vessels that lie in the dura mater and those that lie in the cortex can be identified and are marked in Fig. 5. This distinction enables the study of possibly different roles played by meningeal and cortical vessels in migraine.

Fig. 6 shows the vascular response of one dural vessel, and one cortical vessel of the same animal brain averaged across four trials. The experimental protocol was the same as in Section 2. The differences in the vascular responses of dural and cortical vessels are tabulated in Table 2. In comparison to the 40 ± 8% vasodilatation of the dural vessel, the cortical vessel did not show any change in size during or after the electrical stimulation of the trigeminal nerve fibers. This lack of response was consistent among all six animals. Both vessels showed increased blood velocity in response to the electrical stimulation. However, the cortical vessel showed a faster (mean rate of increase 94% per second vs. 67% per second) and higher (65 ± 5% vs. 50 ± 5%) increase in blood velocity when compared to the dural vessel.

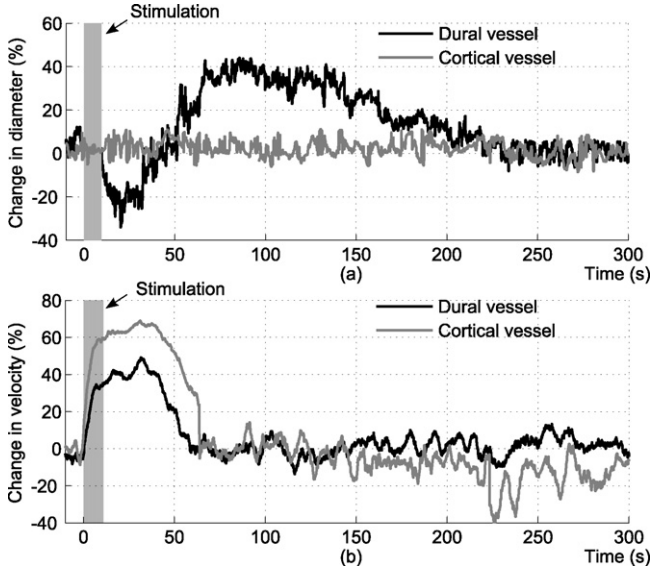

Fig. 6. Contrasting dural and cortical responses to electrical trigeminal stimulation. (a) Mean changes in vessel diameter in dural (black trace) and cortical (grey trace) vessels. (b) Mean changes in blood velocity in dural (black trace) and cortical (grey trace) vessels. While cortical vessels show no change in diameter, they have a larger and faster change in blood velocity compared to the dural vessels (data summarized in Table 2).

4. Discussion and conclusions

We have presented a technique that allows, for the first time, simultaneous measurements of vasomotor and blood flow responses to electrical stimulation of the peripheral trigeminal system which is an accepted model for migraine research. The tLSI method maps blood velocity to contrast without degrading spatial resolution and provides contrast enhanced images of vascular structure. Combining the tLSI and ridge tracking method for vessel size detection, we obtained the blood flow response which is a truer measure of neurovascular interactions rather than the often cited blood velocity (Ayata et al., 2004; Cheng et al., 2003; Paul et al., 2006). In order to compensate for the loss of temporal information during tLSI contrast computation, we proposed and used a sliding window along the time sequences of images that makes the temporal resolution dependent on the camera frame rate alone. The tLSI technique surpasses intravital microscopy (Williamson et al., 2001) in terms of temporal resolution and in simultaneously providing blood velocity measurements. While the image analysis and flow calculations in this work were performed offline, given the simplicity of Eqs. (1)–(3), the technique lends itself to online computation and real-time display. We observed different dynamics in the vasomotor and blood flow responses. The vasomotor activity may be related to the trigeminal nerve innervations, possibly caused by the release of vasodilators like CGRP (Edvinsson and Goadsby, 1994a; Goadsby et al., 2002) while the changes in blood velocity reflect the changes in blood circulation due to the stimulation. The vasomotor dynamics consistently showed a short initial constriction before the larger vasodilation occurred. A similar result has been observed in studies on pig skin (Bartho et al., 1992). Pharmacological studies in that work indicate that the preconstriction is due to the activation of sympathetic fibers. While our observation may have a similar mechanism, further work is

Table 2
Comparison of responses of dural and cortical vessel detected simultaneously using tLSI ($n = 4$ trials).

Parameter	Dural vessel	Cortical vessel
Change in blood velocity		
Mean rate of increase	67% per second	94% per second
Peak magnitude	50 ± 5%	65 ± 5%
Change in vessel diameter		
Mean rate of increase (after constriction)	1.4% per second	No observable changes
Peak magnitude	40 ± 8%	No observable changes

needed to explore the underlying cellular and molecular basis. The non-scanning, wide-field nature of the technique allowed the recording of spatial variations in the response relative to the point of stimulation. We confirmed the expected result that the dynamics would be faster and stronger at vessels proximal to the stimulation location. Responses from different locations along the same branch of the vessel showed the same dynamics. One explanation for this may be that the trajectories of peripheral trigeminal nerve fibers are distributed parallely to the dural vessels (Strassman et al., 2004).

In spite of the inherent two-dimensional nature of tLSI, we demonstrate that the penetration depth of the laser used was sufficient to image dural as well as cortical vessels through a thinned skull in a minimally invasive fashion. This enabled the isolation of responses from vessels in the dura and in the cortex. Contrasting results were seen from dural and cortical vessels. While cortical vessels did not show any vasomotor activity, they showed a stronger and faster blood flow increase compared to dural vessels. This could be due to vasomotor changes being locally mediated via the release of vasodilators and blood flow changes being mediated at higher centers.

In conclusion, tLSI is a minimally invasive imaging modality that offers structural and functional information from the vasculature with high spatiotemporal resolution. It does not need any contrast agents and requires a simple and inexpensive setup consisting of a camera and a ordinary red laser. The non-scanning, wide-field nature of the technique allows recording the vascular dimensions, blood velocity and blood flow over large areas limited only by the optics and the image sensor. The penetration depth of the laser is enough to image both dural and the underlying cortical vessels allowing the distinction of the vessel responses based on which layer they are located in. These features make tLSI a powerful tool in understanding mechanisms involved in neurovascular coupling and in conditions where the coupling may be imbalanced, e.g. migraine.

References

Ahn A, Goadsby P. Animal models of headache. Lippincott Williams & Wilkins; 2006.

Arulmozhi DK, Veeranjaneyulu A, Bodhankar SL. Migraine: current concepts and emerging therapies. Vascul Pharmacol 2005;43:176–87.

Ayata C, Dunn AK, Gursoy OY, Huang Z, Boas DA, Moskowitz MA. Laser speckle flowmetry for the study of cerebrovascular physiology in normal and ischemic mouse cortex. J Cereb Blood Flow Metab 2004;24:744–55.

Aylward S, Pizer S, Bullitt E, Eberly D. Intensity ridge and widths for tubular object segmentation and description. In: Proceedings of math. methods in biomed. Image analysis; 1996. p. 131–8.

Aylward SR, Bullitt E. Initialization, noise, singularities, and scale in height ridge traversal for tubular object centerline extraction. IEEE Trans Med Imaging 2002;21:61–75.

Bartho L, Ernst R, Pierau FK, Sann H, Faulstroh K, Petho G. An opioid peptide inhibits capsaicin-sensitive vasodilatation in the pig's skin. Neuropeptides 1992;23:227–37.

Bergerot A, Holland PR, Akerman S, Bartsch T, Ahn AH, MaassenVanDenBrink A, et al. Animal models of migraine: looking at the component parts of a complex disorder. Eur J Neurosci 2006;24:1517–34.

Briers J. Laser Doppler and time-varying speckle: a reconciliation. J Opt Soc Am A 1996:13.

Briers JD. Laser Doppler, speckle and related techniques for blood perfusion mapping and imaging. Physiol Meas 2001;22:R35–66.

Cheng H, Luo Q, Zeng S, Chen S, Cen J, Gong H. Modified laser speckle imaging method with improved spatial resolution. J Biomed Opt 2003;8:559–64.

De Visscher G, Haseldonckx M, Flameng W. Fluorescent microsphere technique to measure cerebral blood flow in the rat. Nat Protoc 2006;1:2162–70.

Dunn AK, Bolay H, Moskowitz MA, Boas DA. Dynamic imaging of cerebral blood flow using laser speckle. J Cereb Blood Flow Metab 2001;21:195–201.

Edvinsson L, Goadsby P. Neuropeptides in migraine and cluster headache. Cephalalgia 1994a;14:320–7.

Edvinsson L, Goadsby PJ. Neuropeptides in migraine and cluster headache. Cephalalgia 1994b;14:320–7.

Goadsby PJ, Lipton RB, Ferrari MD. Migraine—current understanding and treatment. N Engl J Med 2002;346:257–70.

Goodman JW. Some fundamental properties of speckle. J Opt Soc Am 1976;66:1145–50.

Hillman EM. Optical brain imaging in vivo: techniques and applications from animal to man. J Biomed Opt 2007;12:051402.

Murari K, Li N, Rege A, Jia X, All A, Thakor N. Contrast-enhanced imaging of cerebral vasculature with laser speckle. Appl Opt 2007;46:5340–6.

Ohtsubo J, Asakura T. Velocity measurement of a diffuse object by using time-varying speckles. Opt Quant Electron 1976;8:523–9.

Paul JS, Luft AR, Yew E, Sheu FS. Imaging the development of an ischemic core following photochemically induced cortical infarction in rats using Laser Speckle Contrast Analysis (LASCA). Neuroimage 2006;29:38–45.

Penfield W. Dural headache and innervation of the dura mater. Arch Neurol Psychiatr 1940;44:43–75.

Pietrobon D, Striessnig J. Neurobiology of migraine. Nat Rev Neurosci 2003;4:386–98.

Ray B, Wolff H. Experimental studies on headache: pain sensitive structures of the head and their significance in headache. Arch Surg 1940;41:813–56.

Ruth B. Measuring the steady-state value and the dynamics of the skin blood flow using the non-contact laser speckle method. Med Eng Phys 1994;16:105–11.

Shimazawa M, Hara H. An experimental model of migraine with aura: cortical hypoperfusion following spreading depression in the awake and freely moving rat. Clin Exp Pharmacol Physiol 1996;23:890–2.

Strassman AM, Levy D. Response properties of dural nociceptors in relation to headache. J Neurophysiol 2006;95:1298–306.

Strassman AM, Raymond SA. On the origin of headaches. Endeavour 1997;21:97–100.

Strassman AM, Weissner W, Williams M, Ali S, Levy D. Axon diameters and intradural trajectories of the dural innervation in the rat. J Comp Neurol 2004;473:364–76.

Tamaki Y, Araie M, Kawamoto E, Eguchi S, Fujii H. Noncontact, two-dimensional measurement of retinal microcirculation using laser speckle phenomenon. Invest Ophthalmol Vis Sci 1994;35:3825–34.

Weber R, Ramos-Cabrer P, Hoehn M. Present status of magnetic resonance imaging and spectroscopy in animal stroke models. J Cereb Blood Flow Metab 2006;26:591–604.

Williamson D, Hill R, Shepheard S, Hargreaves R. The anti-migraine 5-HT 1B/1D agonist rizatriptan inhibits neurogenic dural vasodilation in anaesthetized guinea-pigs. Br J Pharmacol 2001;133:1029–34.

Wintermark M, Sesay M, Barbier E, Borbely K, Dillon WP, Eastwood JD, et al. Comparative overview of brain perfusion imaging techniques. Stroke 2005;36:e83–99.

Yu Y, Acton ST. Speckle reducing anisotropic diffusion. IEEE Trans Image Proc 2002;11:1260–70.

Yuan S, Devor A, Boas DA, Dunn AK. Determination of optimal exposure time for imaging of blood flow changes with laser speckle contrast imaging. Appl Opt 2005;44:1823–30.